Studies of Beam Heating of NuMI
Proton Beam Profile Monitors

Thomas H. Osiecki, Sacha E. Kopp, Zarko Pavlovic
University of Texas at Austin

Abstract

We present calculations of the expected temperature rise of the NuMI beam profile monitors due to beam heating. The profile monitors are secondary emission monitors (SEM's) to be made of either Titanium foils or Carbon wires. The heating results in results in potential loss of tension or alignment of the device, and potentially leads to signal degradation. Additionally, calculations of thermally-induced dynamic stress are presented.

1 Introduction

Secondary emission monitors (SEM's) will be located in the vacuum of the accelerator beamline and are to be used to measure the NuMI primary beam profile and halo. A total of 10 monitors are to be located along the primary beam line. The monitors must be sensitive to beam spots of order 1 mm and be accurate in beam centroid measurements to within 50 μm.

Secondary electron emission is a surface phenomenon in which 20-100 eV electrons are ejected from a metal through which passes a charged particle [1]. Such emission occurs with great frequency for highly charged, slow moving charged particle beams, but decreases to approximately 1-5% of an electron per multi-GeV proton[2]. SEM devices may be used at the Main Injector, however, because of the large 4×10^{13} protons/pulse expected will result in a large detectable ejected charge from the SEM.

The NuMI profile monitors will consist of X and Y planes, each of which is segmented into strips or wires. In this way, the relative secondary electron emission from each strip or wire within a plane is a measure of the relative beam intensity across the transverse dimensions of the beam. Presently, two designs are under consideration: a SEM plane consisting of wires as would be in a wire chamber, and a SEM plane consisting of a very thin foil which is segmented into strips.

Low-mass materials are being investigated for the NuMI SEM devices. Three factors motivate the use of low-Z materials. First, the number of interaction lengths of material placed in the beam results in beam loss, and such losses cause increased activation of accelerator components and also of surrounding ground water. Second, the interaction of beam particles in the SEM materials causes heating of the device which results in thermal expansion of the

material and loss of alignment of the strips/wires. Third, thermally-induced dynamic stress in the SEM material may be responsible for signal degradation.

This note procedes as follows: Section 2 discusses the method of the calculation of beam heating used in this note. Section 3 studies the relative beam heating expected as a function of thickness of the SEM material in the beam, and also as a function of the SEM candidate materials. Section 4 uses the expected temperature rise to predict the elongation and tension loss in the SEM planes. Section 5 again uses the expected temperature rise to estimate the temperature stress. Finally in section 6 results of simulations with MiniBoone and 400 MeV Linac proton beam parameters are given.

2   Method

The temperature rise of the SEM's in the beam arises because the power input to each plane from beam energy loss in the material exceeds the power dissipated by conduction of heat to the ends of the strips/wires and the power dissipated via blackbody radiation by the SEM to the walls of the beamline vacuum chamber. The temperature rise of the SEM is given by

$$mC_p\Delta T = \Delta Q = P_{net}\Delta t$$

where m is the mass of a SEM plane, C_p the heat capacity of the SEM material in the beam, ΔT is the temperature rise, ΔQ is the net energy input within a time increment Δt, which is given by $\Delta Q = P_{net}\Delta t$, with the net power input to the SEM given by:

$$P_{net} = P_{beam} - P_{blackbody} - P_{conduction}$$

In this calculation convective cooling and conduction of heat through the air are neglected since the accelerator pipe is evacuated to 10^{-8} Torr.

The beam heating, and consequently the cooling power as well, vary greatly over the surface of the SEM plane. Consequently, we consider the center-most strip or wire in the SEM plane, where the gaussian-peaked beam strikes with greatest intensity. Furthermore, the 12 cm long strip/wire is divided into 1000 cells along its length, and the above heat balance equation applied separately to each cell. This finite element calculation is carried out for multiple successive time increments $\Delta t = 10\mu sec$ until thermal equilibrium is achieved. It is assumed that the vacuum chamber walls and also the ends of the SEM strips/wires are held at $T_{ambient} = 25°C$. A view of a single SEM strip/wire is shown in Figure 1.

In all our simulations, we considered a constant $dx = 200\mu m$ for foil strips, while dx and dz are given by the wire radius r_{wire}, which will be a varied parameter in our simulations. In the case of foil strips, only the thickness dz is varied. The cell length $\Delta y = 0.12mm$ is the same in all simulations.

2.1   Beam Heating

The energy deposited by the beam is calculated from the energy loss by ionization expected for a 120 GeV proton. However, using just Bethe-Bloch formula to calculate the proton
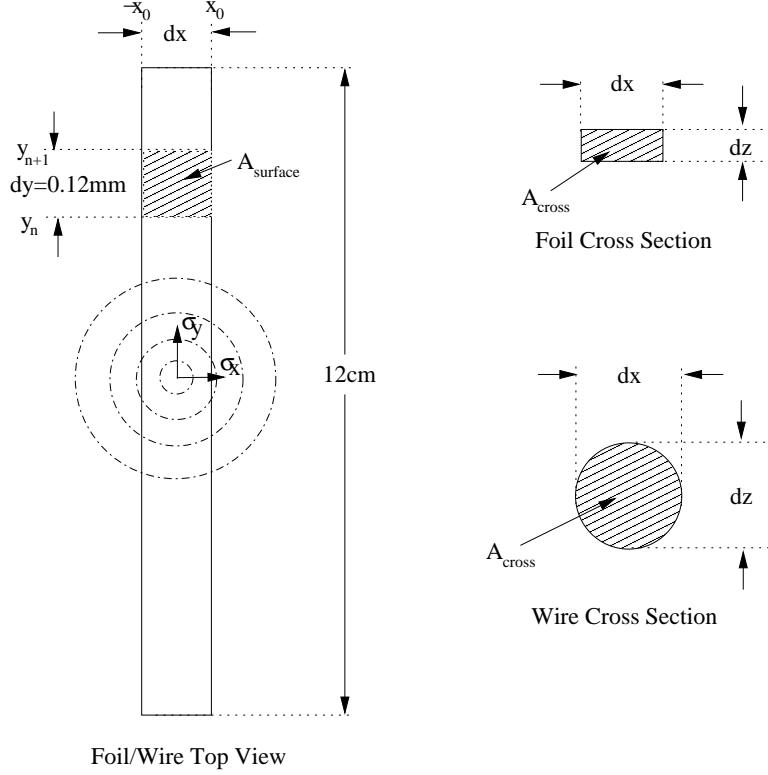
Figure 1: Foil/Wire Dimensions and Variables. (left) Beam's eye view of one SEM strip or wire, indicating the beam spot superimposed, and the definition of one cell along the length of the strip/wire. (right) top or cross sectional view of the SEM strip or wire. The z coordinate runs along the beam direction, and x and y are transverse to the beam. The y coordinate runs along the strip/wire length, with $y = 0$ at one end of the 12cm long strip. The x coordinate is perpendicular to the strip length, with $x = 0$ at the center of the strip width. For a wire, $dx = r_{wire}$ is varied, while for a strip $dx = 200\mu$m is assumed throughout.

energy loss and then taking that as a deposited energy would be an over estimate. For thin foils and wires, energetic δ-rays or "knock-on" electrons, which are liberated in the SEM may escape altogether, so that the energy lost by the beam particles through dE/dx may not all be absorbed in the foil. For this reason we use the restricted energy loss formula to estimate the energy deposited by the proton inside the SEM:

$$-\left(\frac{dE}{dz}\right)_{T<T_{cut}} = Kz^2\frac{Z}{A}\frac{1}{\beta^2}\left[\frac{1}{2}\ln\frac{2m_ec^2\beta^2\gamma^2T_{cut}}{I^2} - \frac{\beta^2}{2}\left(1 + \frac{T_{cut}}{T_{max}}\right) - \frac{\delta}{2}\right] \tag{1}$$

Here the energy transfer is restricted to kinetic energies that are less than some T_{cut}. Details of calculating restricted energy loss are given in appendix A. To estimate T_{cut} we use tabulated range data for electrons [8], and select T_{cut} to be the kinetic energy of an electron

3

| Material | $-\frac{dE}{dx}\left[\frac{MeV}{gcm^{-2}}\right]$ | Foil | | Wire | |
		$T_{cut}[MeV]$	$-\left(\frac{dE}{dx}\right)_r\left[\frac{MeV}{gcm^{-2}}\right]$	$T_{cut}[MeV]$	$-\left(\frac{dE}{dx}\right)_r\left[\frac{MeV}{gcm^{-2}}\right]$
Beryllium	2.03	0.013	1.14	0.05	1.23
Carbon	2.26	0.014	1.26	0.05	1.37
Aluminum	2.16	0.015	1.22	0.055	1.32
Titanium	2.02	0.018	1.14	0.07	1.23
Nickel	2.04	0.027	1.15	0.11	1.25
Silver	1.86	0.027	1.05	0.11	1.13
Tungsten	1.67	0.033	0.94	0.14	1.02
Gold	1.67	0.033	0.93	0.14	1.01

Table 1: Energy loss of 120 GeV protons computed using the Bethe-Bloch formula and the restricted energy loss using T_{cut} for $5\mu m$ thick foil and $D = 50\mu m$ wire.

whose range is equal to half the foil thickness (or equal to the wire radius). Comparison of restricted energy loss to standard Bethe-Bloch result is given for $5\mu m$ thick foil and for the wire with diameter $D = 50\mu m$ in table 1.

To find the total energy deposited by the beam passing through some segment of SEM, we need to find the number of protons passing through that segment. For this we assume that the proton beam has gaussian cross section with similar dimensions in both transvers directions, $\sigma_x \approx \sigma_y \approx 1mm$.

The number of protons passing through area $A = w\Delta y$ around the point $x = X$ and $y = Y$, is given with:

$$N_p = N_{tot}\frac{1}{\sqrt{2\pi}\sigma}\int_{X-w/2}^{X+w/2}e^{-x^2/2\sigma^2}dx\frac{1}{\sqrt{2\pi}\sigma}\int_{Y-\Delta y/2}^{Y+\Delta y/2}e^{-y^2/2\sigma^2}dy \tag{2}$$

where w is the width of the wire/strip and $\Delta y = 0.12mm$ is the cell length. If the σ of the beam is such that $\sigma >> w$ and $\sigma >> \Delta y$ then we can approximately write:

$$N_p \approx N_{tot}\frac{1}{\sqrt{2\pi}\sigma}e^{-X^2/2\sigma^2}w\frac{1}{\sqrt{2\pi}\sigma}e^{-Y^2/2\sigma^2}\Delta y \tag{3}$$

For our analysis we want to consider the foil or a wire that is directly in front of the beam so we can look around the X=0 point and finally write:

$$N_p \approx N_{tot}\frac{w\Delta y}{2\pi\sigma^2}e^{-y^2/2\sigma^2} \tag{4}$$

Having the number of the protons passing through the segment and the energy deposited by each proton we can easily find the increase of the temperature by equating this total deposited energy to $mC_p\Delta T$:

$$\Delta Q = mC_p\Delta T = N_p\rho\frac{dE}{dz}d\bar{z} \tag{5}$$

$$\Delta T = \frac{N_p\rho\frac{dE}{dz}d\bar{z}}{\rho V C_p} \tag{6}$$

4

where V is the volume of the cell equal to the area of the cross section A_{cross} times the cell length Δy and $d\bar{z}$ is the effective thickness of the cell. For the foil this effective thickness is equal to the thickness of the foil dz because all of the protons passing through the segment are passing through the same amount of the material. For the wire the thickness of the wire in the middle is $2R$ and it drops to 0 as x goes to $\pm R$. We can easily find the effective thickness $d\bar{z}$:

$$d\bar{z} = 2 \cdot \int_{-R}^{R} \frac{\sqrt{R^2 - x^2}}{2R} dx = 2R\frac{\pi}{4} \tag{7}$$

Now using the equation for number of protons passing through the segment we get:

$$\Delta T = N_{tot} e^{-y^2/2\sigma^2} \frac{w\Delta L}{2\pi\sigma^2} \frac{\frac{dE}{dz} d\bar{z}}{V c_p} \tag{8}$$

For the foil, the volume of the cell $V = wdz\Delta y$ cancels out of temperature rise. The same is true for a wire, since $w\Delta y d\bar{z} = (2R)(\Delta y)(2R\frac{\pi}{4}) = V$

$$\Delta T = \frac{N_{tot} e^{-y^2/2\sigma^2}}{2\pi\sigma^2 C_p} \frac{dE}{dz} \tag{9}$$

A weak volume dependence in ΔT is implicit in Equation 9 due to the restricted energy loss $\frac{dE}{dz}$, which depends on T_{cut}. This dependence is somewhat different for foils and wires.

2.2 Heat Simulation

We need to consider the problem in which the SEM is being periodicaly heated by beam pulses. Cooling between the pulses is predominately due to heat conduction and blackbody radiation. We can write down the differential equation governing the cooling that includes those two terms:

$$\frac{\partial T}{\partial t} = \alpha \nabla^2 T - \frac{\sigma(T^4 - T_{ambient}^4)}{c_p \rho V} \epsilon A_{surf} \tag{10}$$

where ϵ is the surface emissivity, A_{surf} is surface area and α is thermal diffusivity given with:

$$\alpha = \frac{k}{C_p \rho} \tag{11}$$

k is thermal conductivity.

Given the number of protons and the beam profile we can calculate the increase in temperature for each cell along the wire or foil strip. This then gives us initial conditions. On the boundaries the SEM is on ambient temperature. With these boundary and initial conditions we can numericaly solve the differential eqaution for the period of cooling. Then we can again add the heat from the beam and repeat calculation with new initial conditions. We can repeat this until we get to the desired number of proton pulses.
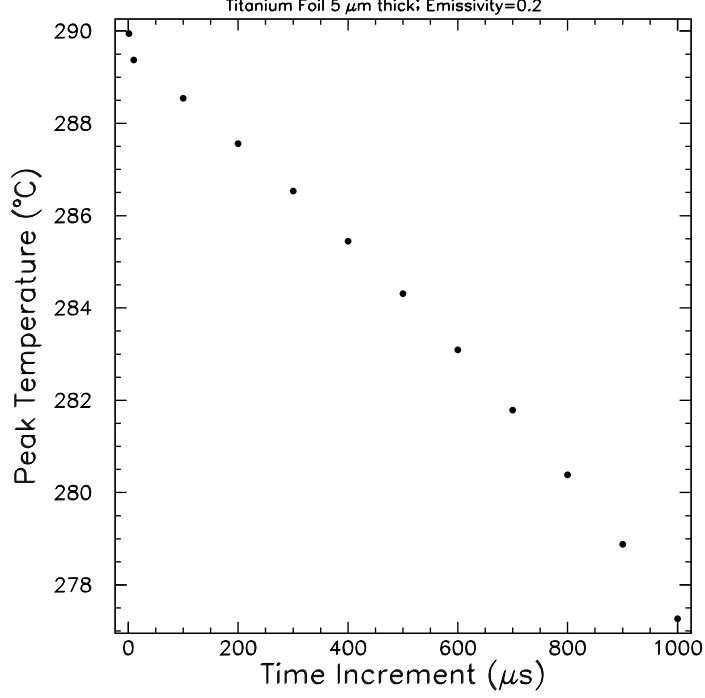
Figure 2: Equilibrium temperature of the center of a SEM strip plotted as a function of the time increment Δt used in the finite element simulation. Note the suppressed zero.

To solve the equation numericaly we need to divide a foil or a wire of length L into N cells. For the i-th cell we can then write:

$$\frac{\partial T_i}{\partial t} = \frac{\alpha}{(\Delta y)^2}(T_{i+1} - 2T_i + T_{i-1}) - \frac{\sigma(T_i^4 - T_{ambient}^4)}{C_p \rho V}\epsilon A_{surf} \tag{12}$$

Our initial conditions for proton pulse n_p are:

$$T_i^{n_p} = T_i^{n_p-1} + \Delta T_i$$

$$T_i^{n_p} = T_i^{n_p-1} + \frac{N_{tot}e^{-(\frac{L}{2}-i\Delta y)^2/2\sigma^2}}{2\pi\sigma^2 C_p}\frac{dE}{dz} \tag{13}$$

with $T_i^{n_p-1}$ being the temperature of the i-th segment just before the next proton pulse and $T_i^0 = T_{ambient}$. The boundary conditions are:

$$T_0 = T_N = T_{ambient} \tag{14}$$

Various parameters for different materials that were considered are listed in Table 2.

As was mentioned before for this simulation we choose to divide the SEM into 1000 cells, so for a 12cm long SEM $\Delta y = 0.012cm$, and for a time increment we choose $\Delta t = 10\mu s$. This

6

Material	Z	Density (g/cm^3) [3]	Heat Capacity (J/g$^\circ$C) [3]	Thermal Conductivity (W/cm$^\circ$C) [3]	Emissivity in Simulation	Emissivity [3]
Beryllium	4	1.848	1.82	2.18	0.1	-
Carbon	6	2.265	0.690	0.24	0.8	0.7-0.8^a
Aluminum	13	2.70	0.899	2.37	0.1	0.04-0.06
Titanium	22	4.54	0.523	0.2	0.2	-
Nickel	28	8.902	0.443	0.899	0.1	0.07-0.09
Silver	47	10.5	0.238	4.27	0.1	0.02-0.04
Tungsten	74	19.3	0.134	1.78	0.1	0.02-0.07^b
Gold	79	19.32	0.130	3.15	0.1	0.03

^{a} graphite ^{b} for temperatures $< 500^\circ$C

Table 2: Properties of candidate SEM materials which enter the calculation of the temperature rise due to beam heating.

value was chosen because smaller time scales greatly increase CPU time to unproductive levels. Yet, from Figure 2, one can see that the equilibrium temperature of the foil at its center approaches an asymptotic value for very small time increments Δt used in the simulation. This variation observed in Figure 2 is due in part to our desire to use very small cell sizes and in part to the fact that the heat due to condution can travel all the way across one cell distance Δy in one time increment if Δt is too long. Figure 2 suggests that the error in the temperature calculations is of the order of a couple of percent due to the choice of $\Delta t = 10\mu$sec. In calculations where time increment was less then the beam spill time, the beam heating was distributed throughout the first $n = \frac{beam\ spill\ time}{\Delta t}$ time increments.

Another motivation to choose a particular Δt comes from the numerical stability condition for heat conduction equation. The stability condition is:

$$\alpha \frac{\Delta t}{\Delta y^2} < \frac{1}{2} \qquad (15)$$

Therefore, since $\alpha < 2cm^2/s$ for all the materials considered, this is satisfied with our choice of Δt and Δy.

During one beam cycle, the impinging beam causes a sharp temperature rise. Following this rise, blackbody radiation and heat conduction allow the foil to cool. This heating and cooling process is evident in Figure 3, which shows the time-development of the temperature at the central cell of a foil strip. The foil is largely able to cool itself within the 1.9 sec beam cycle, leading in this case to temperature cycles of 220°C. Thermal equilibrium, of sorts, is achieved within 15 sec.

The time-evolution of the temperature along the foil's length is shown in Figure 4. Shown is the temperature as a function of position along the length of the strip. Several snapshots over the course of one beam cycle are plotted. The figure is made for the beam cycle which occurs at $t = 26.6\ sec$ in Figure 3. As can be seen, the beam causes a sharp peak in the temperature profile with $\sigma_y \approx \sigma_{beam} = 1$ mm. Later in time, the heat is dissipated by blackbody radiation, reducing the temperature. The heat also flows via thermal conduction to the ends of the strip. This flow is evidenced by the widening peak in the temperature
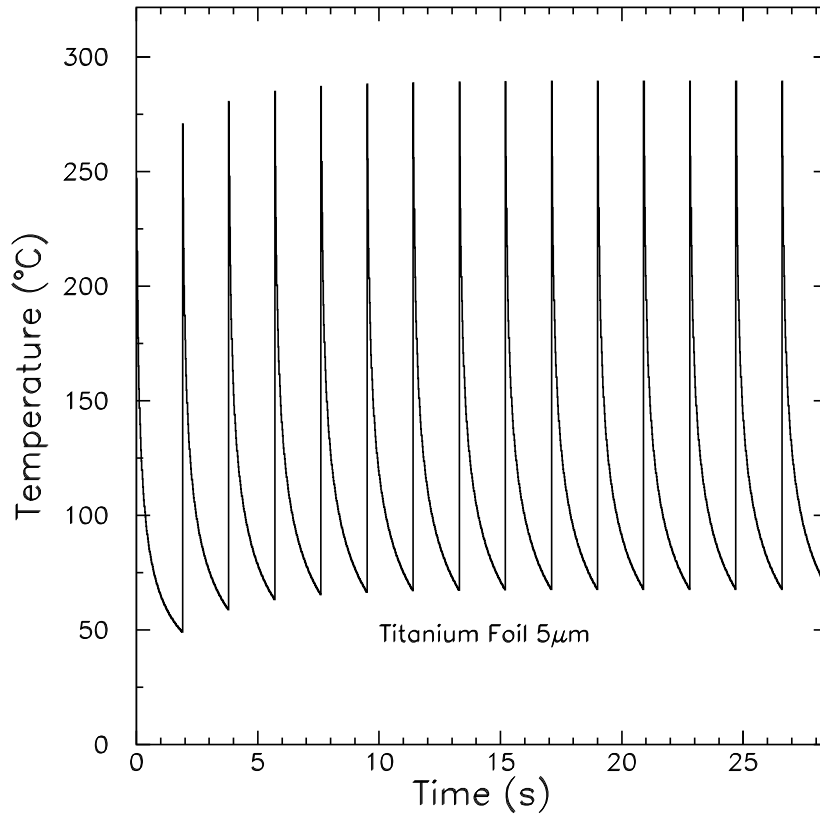
7

Figure 3: Temperature of the center cell of a 5 μm thick Titanium foil as a function of time. The repeated beam cycles each 1.9 sec may be seen as evidenced by the sharp temperature rise.

profile, caused by the flow of heat from the center of the strip at $y = 6$ cm out to the edges which are held at $T_{ambient} = 25°$C. A similar calculation is shown for a 50 μm diameter Ti wire in Figure 5.

Figure 6 shows the results of a simulation which justifies our statement that blackbody radiation is the dominant cooling mechanism for all but the thickest SEM's. The simulation tracks the peak temperature at the center of a foil strip as a function of the thickness of the foil, and the temperature is plotted at equilibrium, immediately before the next beam spill occurs. In this simulation, either blackbody radiation or thermal conduction through the material is successively turned off. It may be seen that for very thin foils, where the surface-to-volume ratio is large, blackbody radiation is clearly more efficient at cooling the foil. Only as the foil thickness grows is the effect of turning off conduction particularly strong. Given that blackbody radiation does dominate, our bias is to consider thin (2-5 μm)
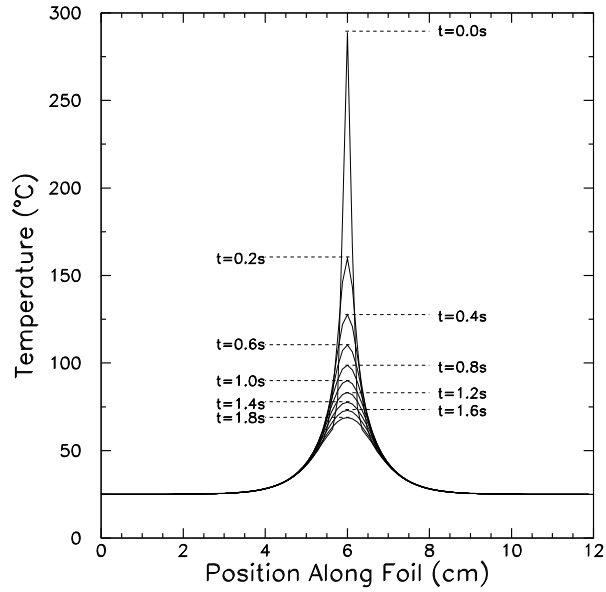
Figure 4: Cooling of a foil from its peak temperature during one beam spill. The beam cycle simulated here occurs at $t = 26.6$ sec in the simulation shown in Figure 3.
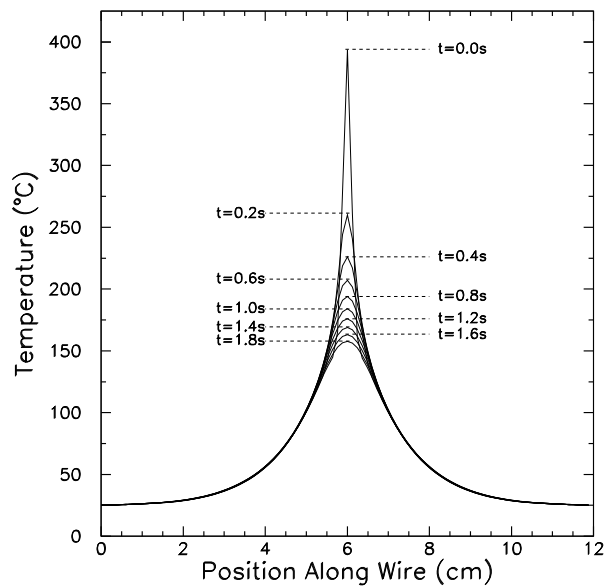

Figure 5: Cooling of a wire from its peak temperature. The simulation is similar to that shown in Figure 4, but is shown here for a 50 μm diameter Ti wire.
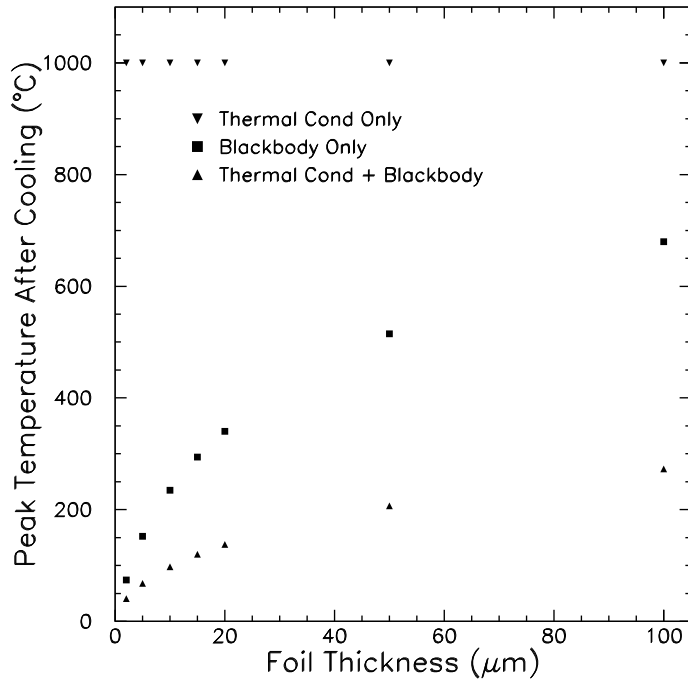
Figure 6: Comparison of different cooling mechanisms on the equilibrium temperature. Shown is the result of a simulation in which beam heating is compensated by either blackbody radiation, by thermal conduction through the strip, or by both these effects.

foils.

3 Alternative SEM Configurations

3.1 Variation of Thickness

The simulations of Titanium wire and foil in Section 2 considered only 5 μm thick foil and 50 μm diameter wire. Thinner foils are possible, albeit with less regularity in the thickness. At 2.5 μm thickness, for example, the variation will be nearly 20%. Thicker foils are readily available as well, and are in general easier to handle. The chemical etching process is easier with thicker parts, although the etching definition is less sharp.

As for wires, the experience at FNAL indicates that very thin wires of order 25 μm (in the case of W-Rh) can become brittle and break after exposure in the beam [9]. Presumably, the breakage occurs because of temperature cycling in the beam. Thus, while thinner wires may place less mass in the beam and hence reduce beam loss, there is a safety limit. There is also past experience at FNAL of wires losing tension after long beam exposure.

10

Figures 7 and 8 show the behaviour of the SEM temperature at the center of a strip/wire as a function of the thickness (foil) or diameter (wire). In each figure are plotted the temperatures in the time increment just after the beam spill has occurred, and also for the time increment just prior to the next beam spill. The values for temperatures are taken from the beam cycle when the "equilibrium" was already reached, so the difference between the peak temperature just after the beam spill and just before the next beam spill is equal to ΔT. From Equation 9 we see that ΔT explicitly depends only on energy deposited in the material and not on the shape of the material, but as was argued before the energy deposited depends on the shape of the SEM through T_{cut}.

The calculations are performed for several possible values of the emissivities, since this quantity is not well known for Titanium (for shiny Aluminum or Gold, the CRC reports a reasonably well-known value of 0.1, but Titanium can be a fair bit 'duller'). Our previous calculations, for example, assumed $\epsilon = 0.2$.

3.2 Variation of Material

In addition to Titanium, other low-Z candidates for either foil or wire SEM's include Be, Al, or C. Beryllium is challenging because of it bio-toxicity. Aluminum is non-ideal because its secondary electron emission signal degrades significantly with beam exposure [2]. However, Carbon filaments have been used by workers at SLAC and Los Alamos [10]. A 30 μm Carbon filament, for example, has about the same beam loss as the 5 μm Titanium foil.

The results of a simulation using different materials is shown in Figure 9. In general, the plot shows the expected rise of foil center temperature with atomic number Z, which is expected due to the increased energy loss by ionization by beam particles in the material (see Table 2). Small variations about this trend, however, are visible. For example, Carbon, while it has an increased temperature just after the spill relative to Beryllium, has a quite low temperature after the 1.9 sec before the next beam spill. This is because it has a large emissivity $\epsilon \sim 0.8$. Aluminum appears to drop below the trend in heating $vs.$ Z, which may well be due to its large thermal conductivity and heat capacity relative to other materials considered (see Table 2).
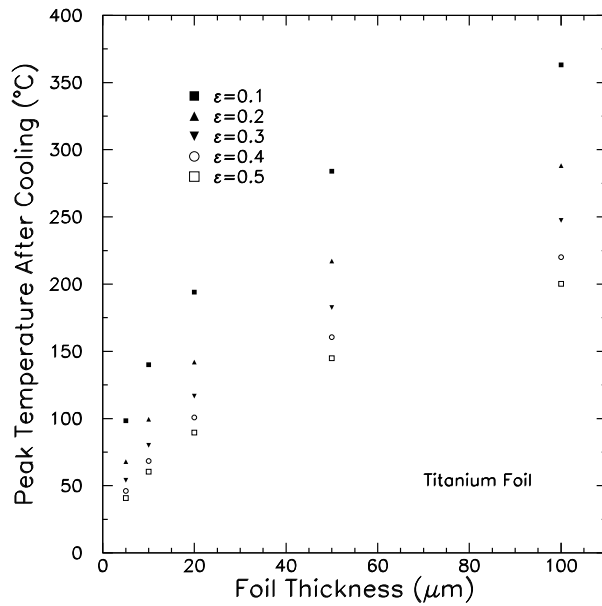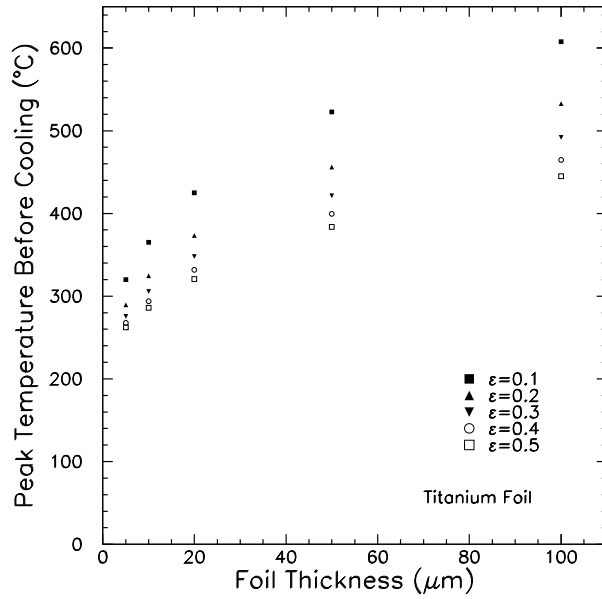
Figure 7: Peak temperature at the center of a Ti foil, shown for several possible emissivities $\epsilon = 0.1 - 0.5$ and several foil thicknesses. (above) Temperature just after a beam spill (below) Temperature just prior to the next beam spill.
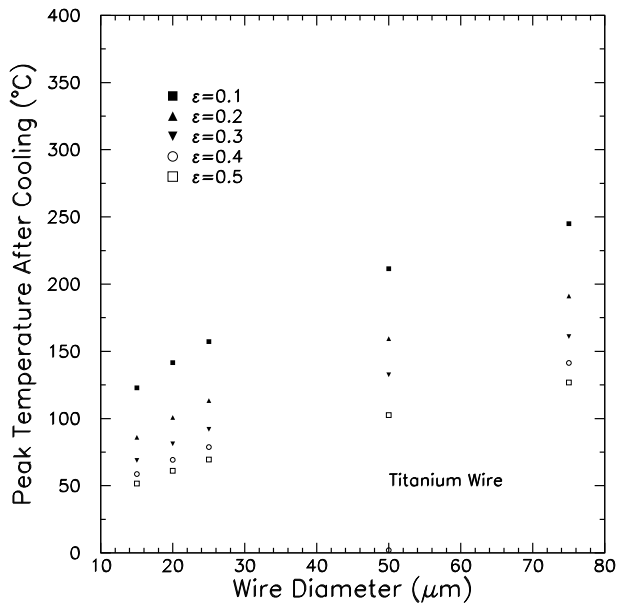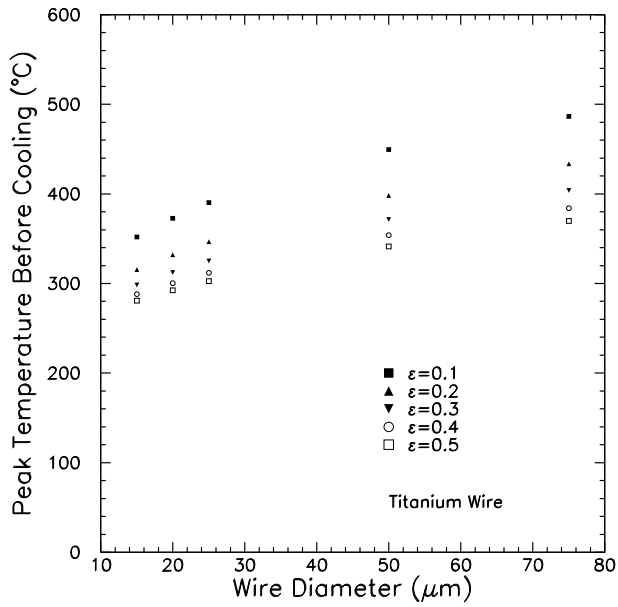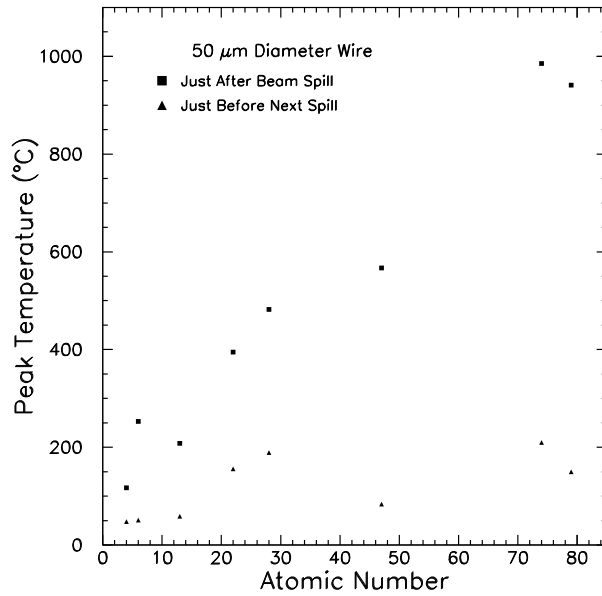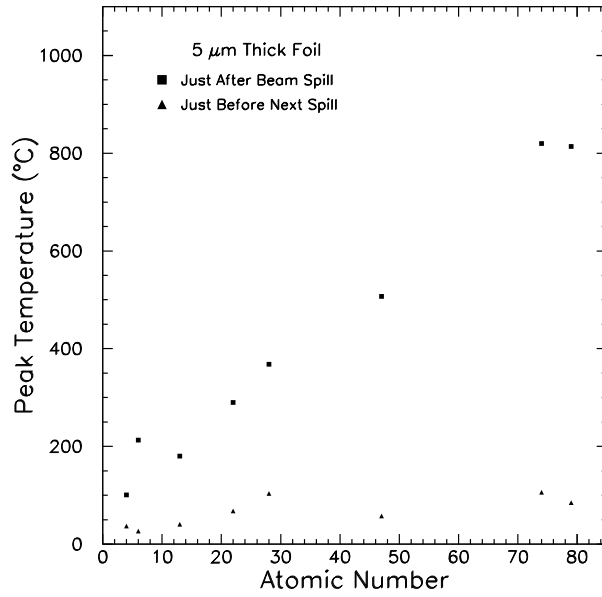
Figure 8: Peak temperature at the center of a Ti wire, shown for several possible emissivities $\epsilon = 0.1 - 0.5$ and several wire diameters. (above) Temperature just after a beam spill (below) Temperature just prior to the next beam spill.

Figure 9: Peak temperature at the center of a strip vs atomic number for 5μm thick foil (above) and 50 μm diameter wire (below) Shown are the peak temperatures just after and just before a beam spill.
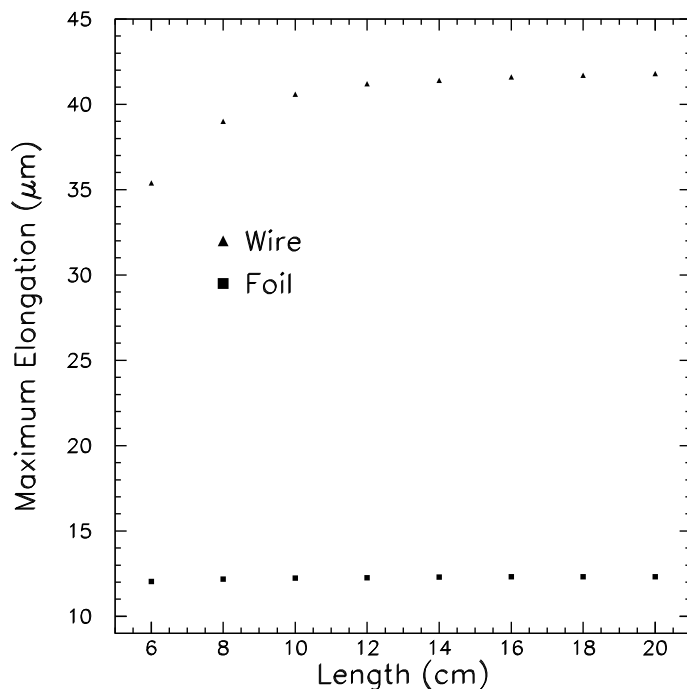
Figure 10: Thermal expansion of a 50μm diameter Ti wire and a 5μm thick Ti foil as a function of the length of the strip/wire. Note the suppressed zero.

3.3 Variation of Length

The length of the strip or wire does not greatly affect the peak temperature at the center of the strip/wire. It does, however, affect the overall elongation of the strip/wire because heat which fails to flow out to the ends of the segment will result in temperature build-up in the "tails" of the peak. This build-up may be noted as the broad gaussian-like profile in Figures 4 and 5. The effect of varying the length is of greater importance for wires, which do benefit by thermal conduction, than it is for thin foils, which dominately cool through blackbody radiation.

In Figure 10 we study the effect of the length of the strip or wire for a Titanium SEM (either 50μm diameter wire or 5μm thick foil). We plot the net elongation (see next section) due to thermal expansion of the strip/wire *vs.* its length. Note that previous simulations have been performed with $L = 12$ cm.
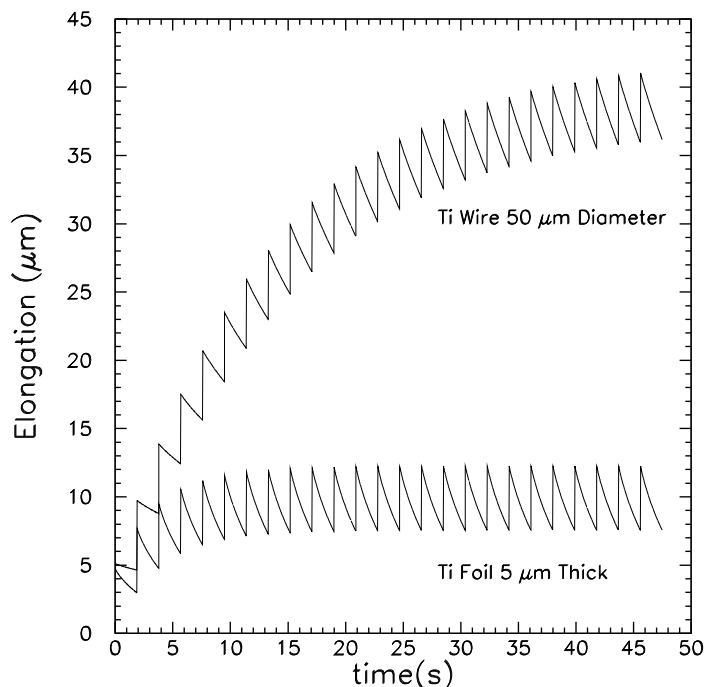
Figure 11: Elongation and Contraction *vs.* time for 120 mm long Titanium 50 μm diameter wire and 5 μm thick foil.

4 Elongation and Tension Loss

The temperature profiles calculated for the many scenarios considered above have been used as the input for the calculation of how much linear expansion is expected due to the net beam heating. The coefficients of thermal expansion for the various materials considered (see Table 3) is multiplied by the cell size dy and the temperature rise from our thermal calculations, and the result summed over the entire length of a strip or wire. Results of calculated linear expansion are shown in Figures 11, 13, and 14.

The results of Figure 11 indicate that the elongation of a 5μm thick foil SEM will result in negligible effects on the strip tension. Foil SEM's, as is discussed in a separate note [13], may be manufactured with accordion-like "springs" pressed into the two ends of the strips. These spring-loaded foils may be pulled over a frame in such a way as to expand by 6-10 mm in the process of stretching the foil SEM on the frame. The resulting tension is of order a couple of grams, sufficient to limit gravitational sag $< 100\mu$m. A schematic sketch of the accordion spring concept is shown in Figure 12.

Inspection of Figure 14 shows that for all materials, a foil SEM has maximum elongation due to beam heating of at most 160μm. For our preferred Titanium foil design, the maximum
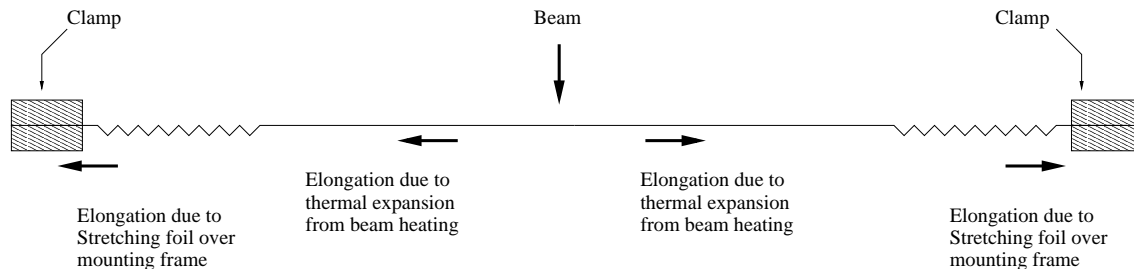
16

Figure 12: Schematic sketch of the accordion springs to be pressed into the foil. The accordion springs are stretched outward by 6-10 mm when the foil is mounted on the frame. Beam heating causes thermal expansion of the foil from the center, which relaxes some of the tension built up in the springs.

elongaton is a modest 12μm. This elongation of 12μm is less then 1% of the elongation used to tension the foil SEM. Thus we conclude that the tension loss of the Titanium foil SEM is of order less then a percent.

The elongation of the SEM wires, in contrast, can result in tension loss. We attempt to estimate this tension loss using the estimated elongation of the wires from Figure 14, assuming that the wires are strung over a frame as is done in conventional wire chamber design, using an applied tension to limit wire sag.

The definition of the Young's modulus is given by

$$E = \frac{L_0}{\Delta L_0} \frac{F}{A}$$

where E is the Young's modulus (in Pascales), L_0 is the original or equilibrium strip/wire length, F is the applied force (in Newtons), A is the cross sectional area of the strip or wire, and ΔL_0 is the elongation of the strip or wire which results from this force F. The linear expansion continues as long as F is less than the yield strength (in Pa) of the material, which is the applied stress under which plastic deformation, or permanent distortion of the material, occurs.

As is well known, wire chambers may be strung only up to a maximum applied tension, lest the wires stretch inelastically and break. For the purposes of our discussion, we take this elastic limit to be the Yield Stress.[1] In Table 3, we have converted Yield Stress to grams of mass that could be used to tension a 50 μm diameter wire, just for the reader's reference. At this maximum tension, there is an elongation to be expected in the wire. From the above definition of the Young's modulus, this elongation is

$$\frac{\Delta L_{max}}{L_0} = \left(\frac{F}{A}\right)_{max} \frac{1}{E} \leq \frac{Y}{E}$$

where Y is defined as the yield stress. This maximum elongagion is tabulated in column 7 of Table 3.
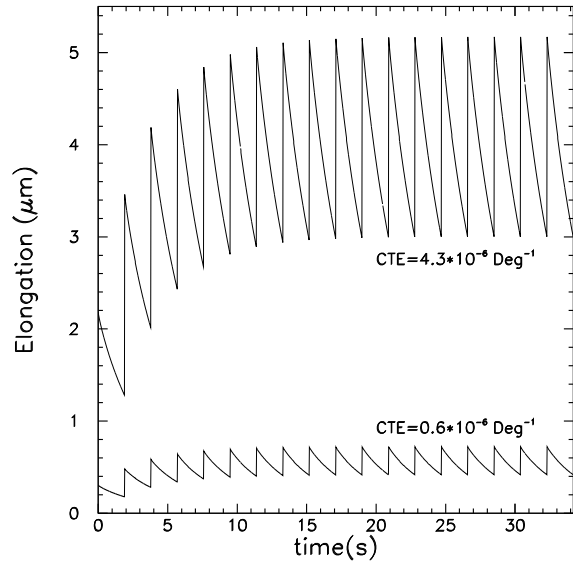
Figure 13: Elongation and Contraction *vs.* time for 120 mm long Carbon 50 μm diameter wire. Because of the range of accepted values for the CTE of Carbon, the calculation was performed with both the maximum and minimum CTE value.
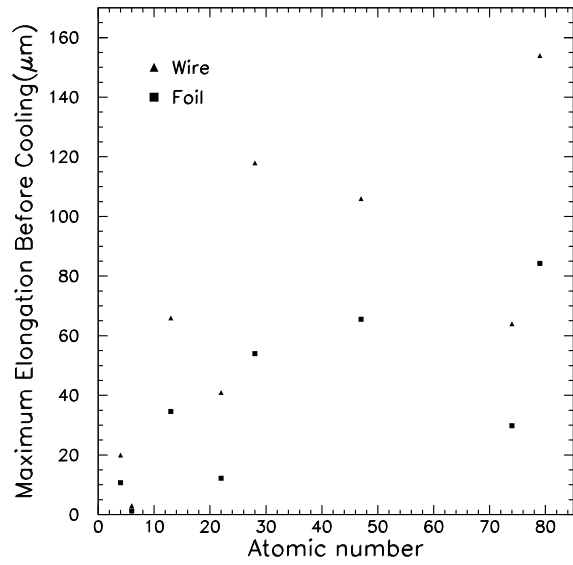

Figure 14: Maximum elongation due to beam heating for strips/wires of 120 mm original length *vs.* the atomic number of the material.

Material	Z	CTE $(10^6/°C)$[3]	Yield Strength [4] (MPa)	(grams)[a]	Young's Mod. (GPa)[4, 5]	Fractional Elongation at Yield Str.$(\times10^{-3})$	Fractional Elongation from Beam Heating $(\times10^{-3})$[a,b]
Beryllium	4	12	240[d]	48	287	0.84	0.17
Carbon	6	0.6-4.3	469[c]	40-45[c]	40.3[c]	11.6	0.025
Aluminum	13	25	10-35[d]	2-7	70.3	0.14-0.50	0.55
Titanium	22	8.5	220[e]	44	115.7	1.9	0.342
Nickel	28	13	1580[d]	316	199.5	7.9	0.983
Silver	47	19	-	-	83	-	-
Tungsten	74	4.5	550[d]	110	411	1.34	0.54
Gold	79	14.2	205[f]	41	82.7	2.48	1.283

[a] For a 50μm diameter wire   [d] soft
[b] Taken from data in Figure 14   [e] annealed
[c] Our measurements of 33μm diameter C monofilaments   [f] hardened

Table 3: Properties of candidate SEM wire materials which enter the calculation of mechanical elongation and loss of tension. The CTE≡"Coefficient of Thermal Expansion". The yield strength, normally expressed in Pascales, is also translated to the gram-equivalent mass which would break a 50μm diameter wire. The fractional elongation at the maximum applied stress (the yield stress) is ≡(Yield Stress)/(Young's Mod.) and is the fractional amount the material would stretch elastically before breaking.

The heating of the wire by the beam results in some loss in tension, or equivalently, a loss in the relative elongation of the wire that is strung over a frame. The beam heating data for 50μm diameter wires in Figure 14, has been tabulated in Table 3. As can be seen, a 50μm Tungsten wire, for example, can lose nearly 40% of its applied tension. The Aluminum wire loses all of its tension.

The present study suggests that the use of springs on individual wires, employed by several workers in the field of beam instrumentation [10, 11], is an important step to ameliorate the effect of beam heating on wire SEM's. Only Carbon wires appear to have a thermal expansion far less than the elongation expected in stringing the wires.

This estimate of tension loss is somewhat over-pessimistic because the elongation of the wire cycles between two values (the maximum just after the beam spill, the minimum just before the next beam spill), and is not equal to the maximum plotted in Figure 14. On the other hand, this estimate underplays the tension loss, since in practice one applies somewhat less than the yield stress to a wire.

---

[1] The actual elastic limit is typically less.

	Foil		Wire		
Material	$\Delta T[^\circ K]$	Dynamic Stress [MPa]	$\Delta T[^\circ K]$	Dynamic Stress [MPa]	Yield Strength
Beryllium	64	188	69	202	240[a]
Carbon	186	19	202	20	469[b]
Aluminum	138	238	150	258	10-35[a]
Titanium	222	208	240	224	220[c]
Nickel	264	736	287	800	1580[a]
Silver	449	709	484	763	-
Tungsten	715	1305	775	1416	550[a]
Gold	729	807	791	877	205[d]

[a] soft   [c] annealed

[b] Our measurements of $33\mu m$ [d] hardened
diameter C monofilament

Table 4: Comparison between dynamic stress and yield strength for a $5\mu m$ thick foil and a $50\mu m$ diameter wire.

5   Dynamic stress

For NuMI, the $8.6\mu s$ proton beam spill time is very short on the time scales involved in heat conduction and blackbody radiation and that is the reason why the temperature rise was mostly treated like the initial condition since in most of the calculations the time increment Δt was greater than the spill length. This, of course, means that there will be a sharp temperature rise in the SEM. This sudden increase in temperature causes a stress in a material given with [12]:

$$S = E\alpha\Delta T \tag{16}$$

where E is the Young's modulus and α is the coefficient of thermal expansion. If this stress is greater than some critical value the material can be deformed or it can even break. As in Section 4 the yield strength can be taken as a comparison.

The maximal stress will be produced in a segment which will heat up the most. Using Equation 9 we can find this ΔT. Tabel 4 lists results for a $5\mu m$ thick foil and $50\mu m$ diameter wire made of various materials and compares them to the yield strength.
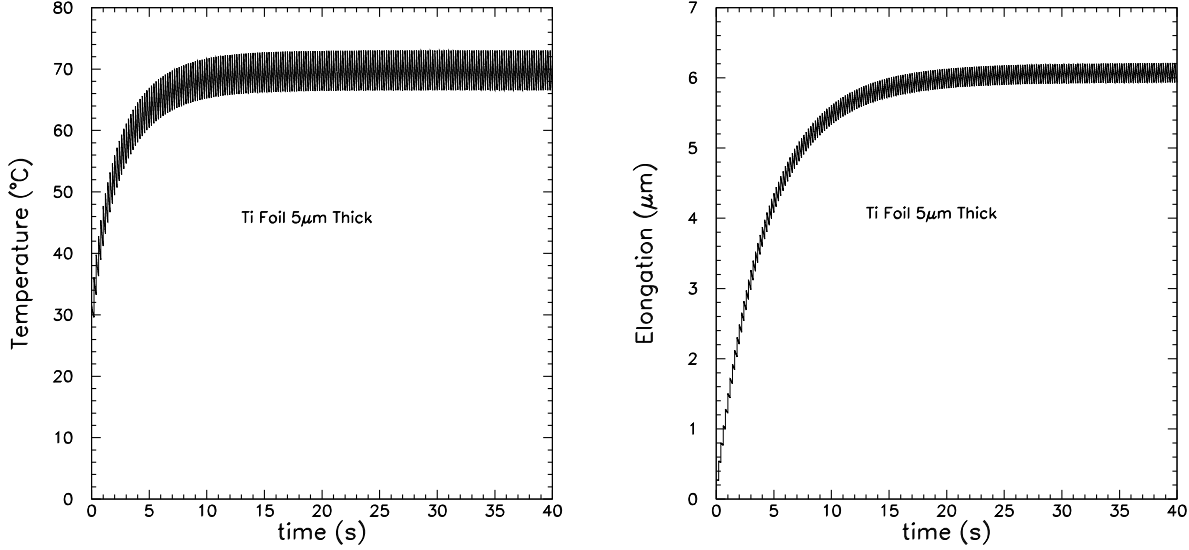
Figure 15: (left) Expected temperature rise at the center of the hottest foil during the upcoming test of the NuMI SEM in the MiniBoone beamline. (right) Net elongaton of the hottest Titanium foil during the MiniBoone test.

6   Calculations for other Beam lines

In Spring 2003 a prototype of the NuMI profile monitor SEM was tested in the MiniBoone transfer line. We estimate here the expected thermal performance of the SEM prototype in this test. We also estimate the thermal performance of the SEM in a 400 MeV linac. A number of differences exist between the $8GeV$ booster, $400MeV$ linac and the NuMI conditions. They are listed below. With these inputs, we estimate the results shown in Figure 15 for the MiniBoone test.

	400 MeV linac	MiniBoone	NuMI
Beam Kinetic Energy (GeV)	0.4	8	120
Spill Length (μs)	25	1.56	8.6
Rep. Rate (Hz)	15	5	0.53
Protons/spill	5×10^{12}	5×10^{12}	4×10^{13}
Spot Size, σ (mm)	~5	~ 2	~ 1

Table 5 lists the results for titanium foil, titanium wire and tungsten wire for the three beam lines. Altough the temperatures are quite different for NuMI beam line and Linac, the fractional elongations are almost the same because the temperature distribution along the foil/wire is different. It is much more broader for Linac than for NuMI. Figure 16 shows the temperature distribution along the foil/wire for Linac and MiniBoone. Again, from these

21

	Thickness/ Diameter[μm]	$-\frac{dE}{dx}\left[\frac{MeV}{gcm^{-2}}\right]$	$T_{max}[^\circ C]$	$\Delta T[^\circ K]$	Fractional elongation[$\times 10^{-4}$]
		400 MeV linac			
Ti Foil	5	1.97	92.5	1.92	1
Ti Wire	50	2.06	191	2	3.9
W Wire	25	1.55	226	5.89	4.1
W Wire	50	1.57	277	5.97	5.4
W Wire	75	1.59	308	6.04	6.3

	Thickness/ Diameter[μm]	$-\frac{dE}{dx}\left[\frac{MeV}{gcm^{-2}}\right]$	$T_{max}[^\circ C]$	$\Delta T[^\circ K]$	Fractional elongation[$\times 10^{-4}$]
		MiniBoone			
Ti Foil	5	1.07	73.1	6.5	0.52
Ti Wire	50	1.16	137	7.1	2.2
W Wire	25	0.9	157	21.4	2.3
W Wire	50	0.93	189	22.1	3.2
W Wire	75	0.94	204	22.3	3.6

	Thickness/ Diameter[μm]	$-\frac{dE}{dx}\left[\frac{MeV}{gcm^{-2}}\right]$	$T_{max}[^\circ C]$	$\Delta T[^\circ K]$	Fractional elongation[$\times 10^{-4}$]
		NuMI			
Ti Foil	5	1.14	290	222	1
Ti Wire	50	1.23	400	240	3.4
W Wire	25	0.99	920	753	4.1
W Wire	50	1.02	990	775	5.4
W Wire	75	1.04	1035	791	6.3

Table 5: Results for $5\mu m$ thick Ti foil, $50\mu m$ Ti wire and 25, 50 and $75\mu m$ W wire for different beam line parameters.

plots we can see that cooling of the foil is almost entirely due to blackbody radiation, there is almost no flux of heat to the boundaries. For the wire we see that the peak is broader and there is some heat flux into the boundaries which contributes somewhat to cooling.
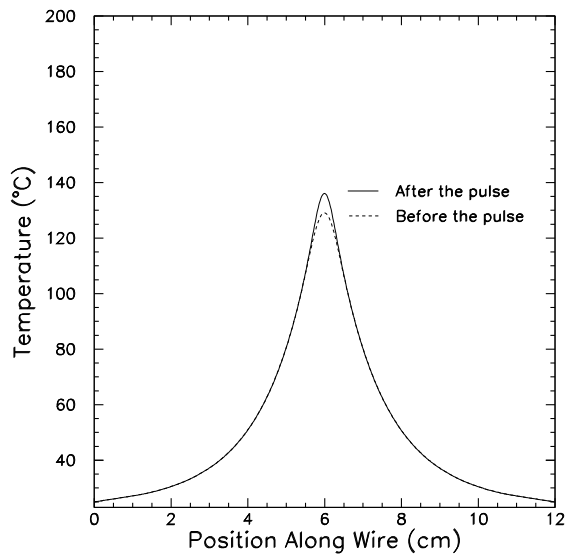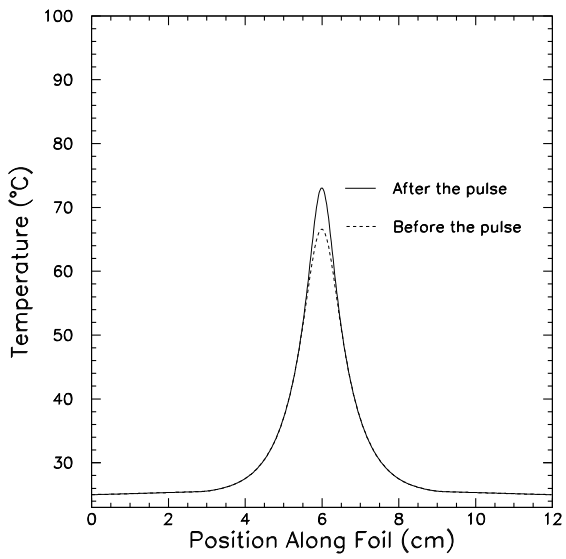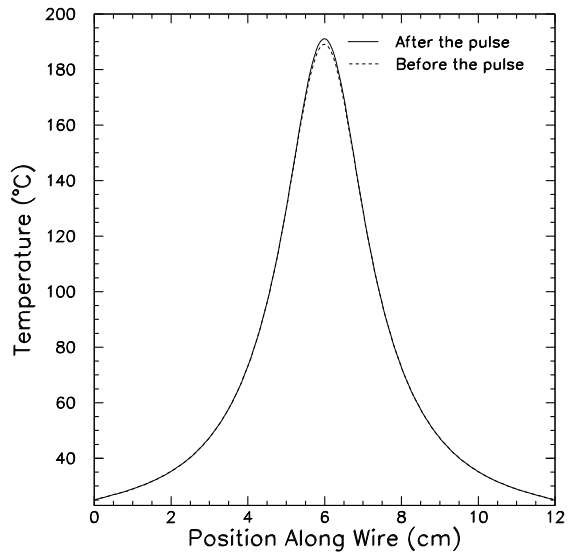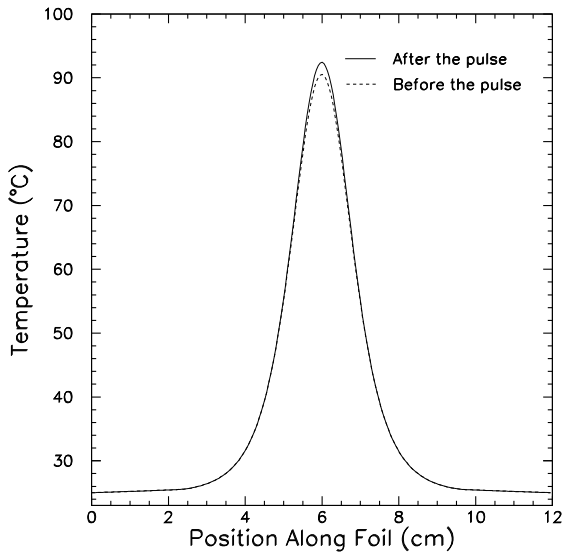
Figure 16: Temperature distribution along the foil/wire after reaching "equilibrium" calculated for Linac (top) and MiniBoone (bottom) beam line parameters.

7   Conclusion

We have performed simulations of the beam heating in vacuum of various candidate SEM materials by the NuMI beam. Our estimates indicate that a Titanium foil SEM experiences acceptably small tension loss, provided that accordion springs in the material are employed to take up the thermal expansion. To keep the tension loss at the few percent level, the accordion springs should be able to accomodate up to 5-7 mm of expansion. Our estimates also suggest that a wire SEM without springs will not operate without tension loss, with the possible exception of a Carbon wire SEM.

References

[1] H.Bruining, "Physics and Applications of Secondary Electron Emission," (London, Pergammon Press), 1954.

[2] G. Ferioli & R. Jung, "Evolution of Secondary Electron Emission Efficiencies of Various Materials Measured in the CERN SPS Secondary Beam Lines," CERN-SL-97-71(B1), talk presented at DIPAC '97.

[3] Handbook of Chemistry and Physics,68th Ed. Ed: Robert C. Weast. CRC Press, 1987-1988.

[4] `http://www.kasap.usask.ca/server/kasap/Tables/Mechanical.html`

[5] Handbook of Physical Quantities. Ed: Igor S. Grigoriev and Evgenii Z.Meilikhov. CRC Press, 1997.

[6] K. Hagiwara *et al.*, "Review of Particle Properties," *Phys. Rev.* **D66**, 010001 (2002).

[7] B. Rossi, *High Energy Particles*, (Englewood Cliffs: Prentice Hall, Inc.) 1952. See especially Section 2.5, equations 2.5.4 and 2.5.6.

[8] National Institutes of Standards and Technologies, "Stopping Powers of Electrons, Protons, and Alpha Particles," `physics.nist.gov/PhysRefData/`.

[9] Gianni Tassotto, FNAL Beam Instrumentation Group, private communication.

[10] R.Valdiviez *et al.*, Proceedings of 2001 Particle Accelerator Conference, p.1324.

[11] J.Krider & C. Hojvat, *Nucl. Instr. Meth.* **A247**, 304 (1986).

[12] R. J. Roark, W. C. Young, "Formulas for Stress and Strain"

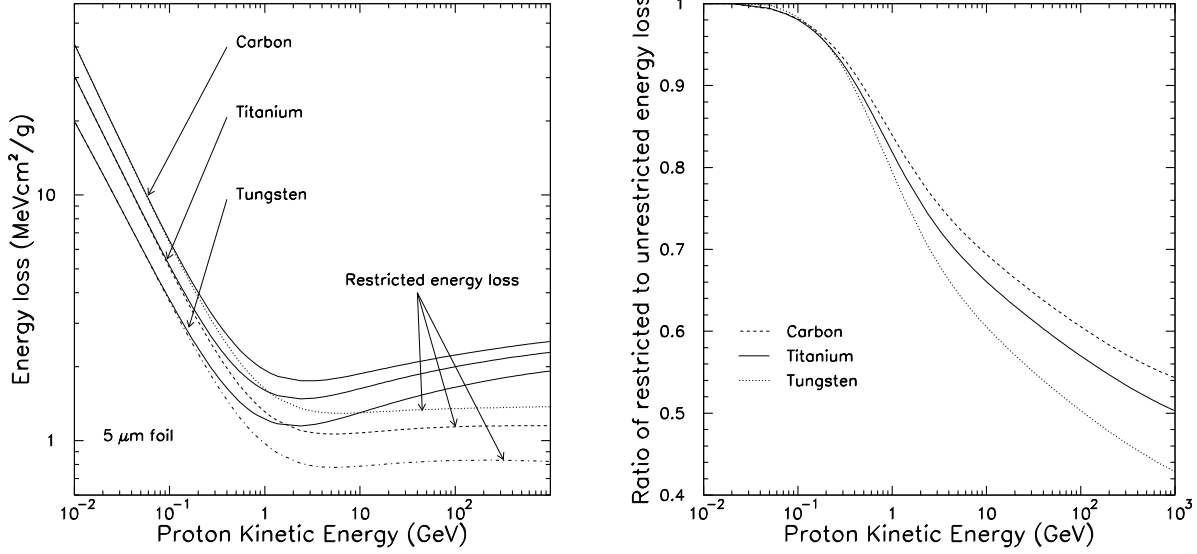[13] Sacha E. Kopp, Marek Proga "Design of The Prototype NuMI Profile Monitor SEM", NuMI-B-933 (2003)

Figure 17: Restricted energy loss compared to unrestricted for $5\mu m$ foil.

A Energy Loss

Moderately relativistic charged particles other than electrons lose energy in matter primarily by ionization and atomic excitation. The mean rate of energy loss (or stopping power) is given by the Bethe-Bloch equation,

$$-\frac{dE}{dx} = K z^2 \frac{Z}{A} \frac{1}{\beta^2} \left[\frac{1}{2} \ln \frac{2m_e c^2 \beta^2 \gamma^2 T_{max}}{I^2} - \beta^2 - \frac{\delta}{2} \right] \qquad (17)$$

Here T_{max} is the maximum kinetic energy which can be imparted to a free electron in a single collision.

Integrating Equation 17 we can find the total 'continuous slowing-down approximation' range R. This is for a particles which loses energy only through ionization and atomic excitation.

For a particle with mass M and momentum $M\beta\gamma c$, T_{max} is given by:

$$T_{max} = \frac{2m_e c^2 \beta^2 \gamma^2}{1 + 2\gamma m_e/M + (m_e/M)^2} \qquad (18)$$

For density effect correction we use Sternheimer's parameterization:

$$\delta = \begin{cases} 2(\ln 10)x - \bar{C}) & x \geq x_1; \\ 2(\ln 10)x - \bar{C} + a(x_1 - x)^k & x_0 \leq x < x_1; \\ 0 & x < x_0 (nonconductors); \\ \delta_0 10^{2(x-x_0)} & x < x_0 (conductors); \end{cases}$$
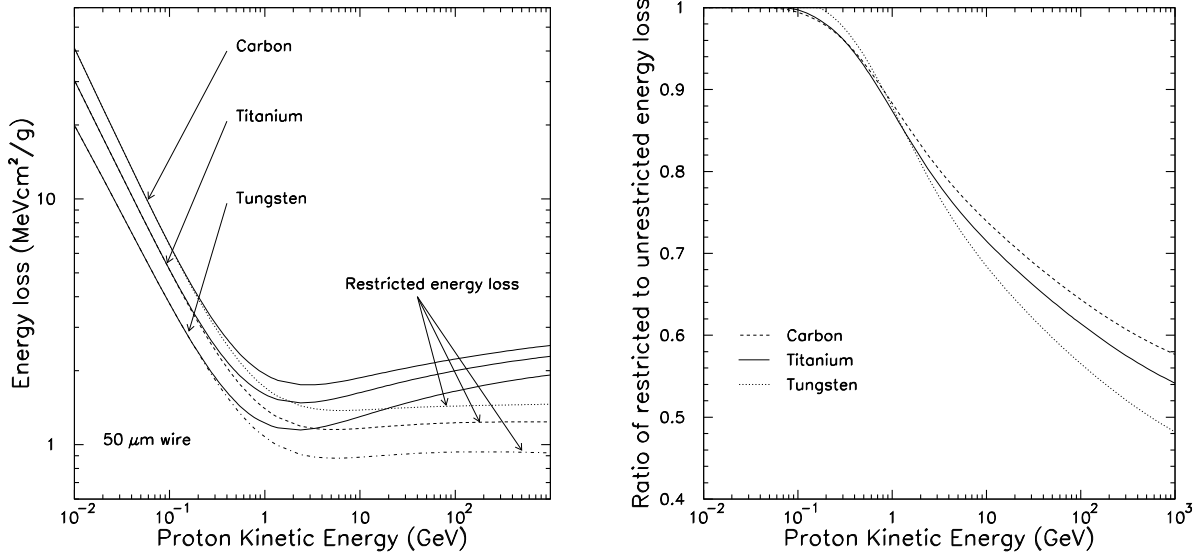
25

Figure 18: Restricted energy loss compared to unrestricted for $50\mu m$ wire.

Here $x = \log_{10}(p/Mc)$. Parameters for various materials considered as SEM candidates are listed in table 6.

Proton passing through the material will deposit energy by ionizing particles. Since we are considering thin foil or wire as a target, only electrons with energy lower than some T_{cut} will stay inside the SEM material. Because of that we need to modify Equation 17. The restricted energy loss rate is:

$$-\left(\frac{dE}{dx}\right)_{T<T_{cut}} = Kz^2\frac{Z}{A}\frac{1}{\beta^2}\left[\frac{1}{2}\ln\frac{2m_ec^2\beta^2\gamma^2T_{cut}}{I^2} - \frac{\beta^2}{2}\left(1 + \frac{T_{cut}}{T_{max}}\right) - \frac{\delta}{2}\right] \qquad (19)$$

Figure 17 and Figure 18 show the restricted and unrestricted energy loss and their ratio. Subtracting Equation 1 from Equation 17 we get the drop in energy deposition due to

Material	a	k	x_0	x_1	$\bar{C}$	δ_0
Beryllium	0.80392	2.4339	0.0592	1.6922	2.7847	0.14
Carbon	0.26142	2.8697	-0.0178	2.3417	2.868	0.12
Aluminum	0.08024	3.6345	0.1708	3.0127	4.2495	0.12
Titanium	0.15662	3.0302	0.0957	3.0386	4.445	0.12
Nickel	0.16496	2.843	-0.0566	3.1851	4.3115	0.1
Silver	0.24585	2.6899	0.0657	3.1074	5.063	0.14
Tungsten	0.15509	2.8447	0.2167	3.496	5.4059	0.14
Gold	0.09756	3.1101	0.2021	3.6979	5.5747	0.14

Table 6: Parameters needed for density corrections.

restricted energy loss:

$$\Delta = K z^2 \frac{Z}{A} \frac{1}{\beta^2} \left[\frac{1}{2} \ln \frac{T_{max}}{T_{cut}} - \frac{\beta^2}{2} \left(1 - \frac{T_{cut}}{T_{max}} \right) \right] \qquad (20)$$